Conference Paper, Published Version

Yeh, Harry; Tonkin, Susan; Heller, Eric; Arduino, Pedro; Kato, Fuminori; Sato, Shinji

Mechanisms Of Scour Induced By Tsunami Runup

MECHANISMS OF SCOUR INDUCED BY TSUNAMI RUNUP*

HARRY YEH
Department of Civil Engineering, Oregon State University
Corvallis, OR 97331, USA

SUSAN TONKIN
Moffatt & Nichol, 710 Second Ave #720
Seattle, WA 98104, USA

ERIC HELLER
GeoEngineers, 600 Stewart St., #1420
Seattle, WA 98101, USA

PEDRO ARDUINO
Department of Civil Engineering, University of Washington
Seattle, WA 98195, USA

FUMINORI KATO
National Institute for Land & Infrastructure Management, 1 Asahi, Tsukuba
Ibaraki 305-804, Japan

SHINJI SATO
Department of Civil Engineering, University of Tokyo, Hongo 7-3-1
Bunkyo-ku, Tokyo 113-8656, Japan

Tsunamis are known to cause substantial scour on shore. The scour mechanisms are expected to be different from those contributing to bridge or pier type scour processes in a river or offshore environment. The scouring associated with tsunami runup occurs in a short duration, less than half an hour, and no equilibrium state is reached. A series of scale model experiments investigated the scouring mechanisms associated with a tsunami impinging on a coastal cylindrical structure. Video images from inside the cylinder elucidated the vortex structures and the time development of scour around the cylinder. For the sand substrate, the most rapid scour occurred at the end of drawdown – after flow velocities had subsided and shear stresses had presumably decreased. This behavior can be explained in terms of pore-pressure gradients. During the tsunami drawdown, the water level subsides and the pressure on the sediment bed decreases, creating a vertical pressure gradient within the sand and decreasing the effective stress. The surface pressure decreases approximately linearly from a sustained peak at ΔP to zero over time ΔT. The critical fraction Λ of the buoyant weight of sediment supported by the pore pressure gradient can be estimated as: $\Lambda = \frac{2}{\sqrt{\pi}} \frac{\Delta P}{\gamma_b \sqrt{c_v \Delta T}}$, in which γ_b is the buoyant specific weight of the saturated sediment and c_v is the coefficient of consolidation. The value of c_v was determined with an unconventional method: by directly measuring the temporal and spatial variations of pore-pressure field in the controlled laboratory apparatus. It was found that much deeper scour results when Λ exceeded one-half for the experiments on scour around a vertical cylinder.

* This work was supported by the US National Science Founation (CMS-9978399) and Public Works Research Institute, the Japan Ministry of Construction.

1 Introduction

Recent tsunami surveys from the 1992 Nicaragua tsunami to the 1998 Papua New Guinea tsunami clearly observed substantial scour effects around structures and trees: see Fig. 1. Tsunami scouring is often the primary cause of structure damages and destruction, as well as uprooting trees on the shore. The 1960 Chilean tsunami scoured out the bed by approximately 10 m at Kesen-numa Port in Japan (Takahashi et al. 1992). Note that typhoons attack the site every several years and the associated wave heights offshore are much higher than the tsunami. Yet, such typhoon-generated waves do not cause such a remarkable scour resulted from the tsunami. For a typical tsunami, the water surface near the shore fluctuates with amplitude of several meters during a period of a few to tens of minutes. This timescale is intermediate between the hours to days typical of slope instability problems associated with rapid drawdown, and the tens of seconds or less associated with cyclic storm-wave loading. Table 1 lists some examples of phenomena known to cause severe scour or soil liquefaction.

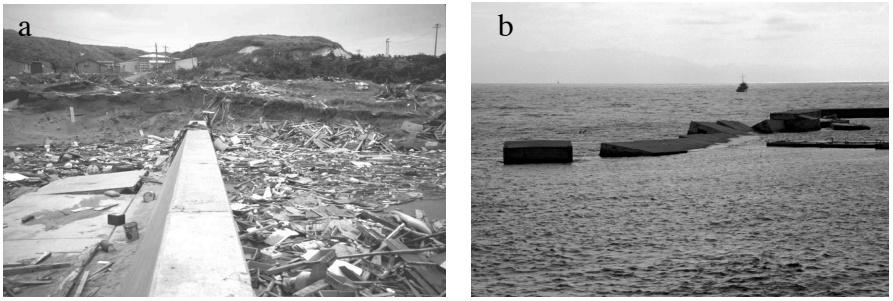

Figure 1. Damage caused by the 1993 Okushiri Tsunamis. a) tsunami scour at Aonae Port; b) foundation failure of the breakwater at Okushiri Port. (Photos by H. Yeh)

Table 1: Geotechnical Scour and Liquefaction Phenomena

Phenomenon	**Time scale**	**Pressure scale (change in head)**	**Comments**
River flood	Hours to days	1 to 10 meters	Scour is associated with fluid velocity rather than pressure changes
Rapid drawdown due to spring tides or dam breaks	Hours	10 meters typical	Pore pressure distribution described using quasi-static consolidation theory
Tsunami	A few to tens of minutes	1 to 10 meters	Transient loading
Wind-generated waves	Tens of seconds	1 meter typical	Cyclic loading
Earthquake	Seconds	N/A	Cyclic loading; liquefaction not caused by change in water level

2. Experiments and analyses

To investigate scouring mechanisms associated with tsunami runup onto a dry beach, a series of scale model experiments were carried out using a large-scale sediment tank (135m long, 2m wide, and 5m deep). A beach of well-graded sand was constructed with a uniform slope of 1:20. A solitary wave was generated offshore as a model of an incident tsunami. A model cylinder, shown in Fig. 2, was placed upright on the beach. The cylinder was 50 cm in diameter, made of 1 cm thick Plexiglas, water tight at the bottom end, and connected above to an aluminum cylinder for stiffness. Taking the advantage of

the transparent cylinder wall, scour processes were recorded from the interior with three miniature CCD video cameras, which cover more than 180-degree view of the circumference from the offshore to inshore sides. To examine the sediment conditions, pore pressure transducers were embedded around the cylinder. Details of the experiments are given in Tonkin et al. (2003).

We observed from the experiments that in the first second after the wave strikes, a large horseshoe-type vortex, originating from the overturning motion of the wave breaking offshore, is set up at the front of the cylinder. Figure 3 shows the observed scour depth at the cylinder wall as a function of time. In this cases — that is cylinder initially at the shoreline, water depth h = 2.45 m, offshore incident solitary-wave height H = 22 cm, H/h = 0.09 — this vortex scours about 7 cm deep. Throughout the runup, the sand scoured from the front and side of the cylinder is brought into suspension and carried away from the cylinder. During the early part of drawdown, little sand is scoured from the back of the cylinder. During the last few seconds of drawdown – the most turbulent period – a strong horseshoe-type vortex forms at the back of the cylinder. A very large quantity of sand is scoured from the back of the cylinder during this period.

Figure 2: Side view of the instrumented cylinder.

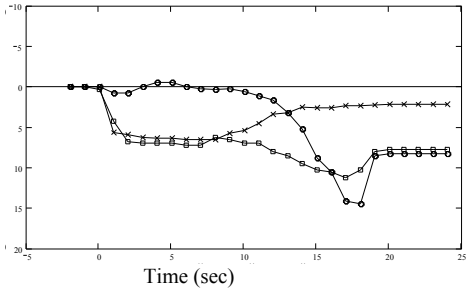

Figure 3: Scour depth (cm) as a function of time. Crosses, at the front; squares, at the side; circles, at the back of the cylinder.

Figure 4 illustrates the Shields parameter θ (dimensionless shear stress) together with the observed scour depth and the rate of scour at the back of the cylinder. The Shields parameter θ was estimated using the formulation in Hoffmans and Verheij (1997):

$$\theta \equiv \frac{\tau}{gD_{50}\left(\rho_s - \rho_W\right)} \approx \frac{1}{gD_{50}} \frac{\rho_w}{\rho_s - \rho_w} \left[\frac{\kappa u}{\ln\left(30z/D_{90}\right)}\right]^2, \qquad (1)$$

where g is the acceleration due to gravity, D_{50} is the median sediment diameter, D_{90} is the 90th percentile of the sediment diameters, ρ_w is the density of water, ρ_s is the sediment grain density, κ = 0.4 is the van Kármán constant and u is the horizontal flow speed at a height z above the surface. The flow velocity u was measured at z = 7.5 cm and 3 meters offshore from the cylinder. Therefore the actual flow velocity (and so the Shields parameter) at the cylinder lags the measured velocity during runup, and may lead the measured velocity during drawdown. The origin of the time scale has been shifted (by less than one second) to account for the phase lag during runup.

Figure 4 demonstrates that the shear stress peaks near t = 0, when the wave first reaches the cylinder; this is reflected by rapid scour at the front of the cylinder. Little scour occurs at the back of the cylinder at t = 0 due to the shadowing caused by the cylinder. The shear stress has another peak during drawdown, at between 10 and 16 s.

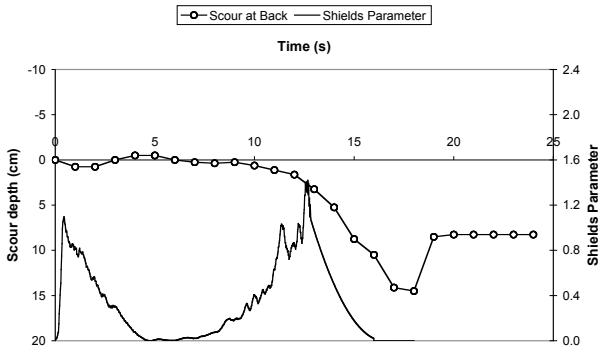

Figure 4: Measured scour depth and estimated Shields parameter for the case of cylinder initially at the shoreline, water depth h = 2.45 m, offshore incident solitary-wave height H = 22 cm, H/h = 0.09.

The flow velocity, and consequently the shear stress, drop to zero in the 2-3 s following this peak. Most of the scour at the back of the cylinder occurs at between 14 and 17 s. During this time, the estimated shear stress is dropping rapidly and the sediment load transported from further onshore is observed to be increasing – so the scour rate would be expected to decrease. The main discrepancy between the predictions of the shear stress model and the observed scour rate is that the scour rate reaches its maximum at between 16 and 17 s – just as the flow velocity drops to zero!

Figure 5 shows a visibly liquefied soil state at the final state of tsunami drawdown. Note that at this stage, the scour action cannot be explained by the flow shear stress, since the flow had been diminished to almost nil. This basic observation casts doubt on the adequacy of the shear stress approach. Our hypothesis to explain the significant scour effects caused by tsunamis is that the temporal and spatial variations in pore-pressure within soils might cause weakening in the structure of the soil skeleton. In particular, as the water level subsides, the pressure on the sediment bed decreases, creating a vertical pressure gradient within the soil and decreasing the effective stress within the soil. This results in scour enhancement although the scour itself is, of course, driven by the surface shear stresses induced by the rapid tsunami flow.

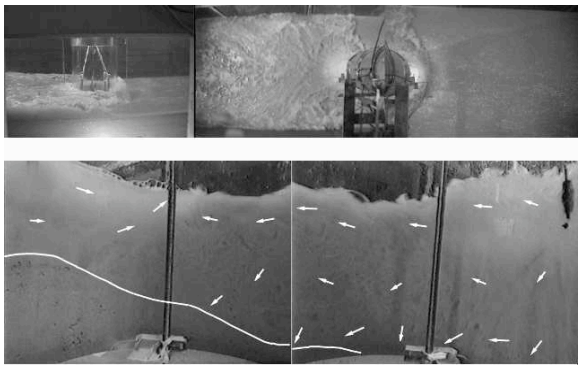

Figure 5. Video imagery showing soil liquefaction around the cylinder observed at the end of tsunami drawdown. The upper right-hand panel was recorded from directly above the cylinder. The wave is running down from right to left. The two lower panes were recorded from inside the cylinder. The arrows are used to illustrate the flow field and the line indicates the stationary sediment surface. The upper left-hand pane is a side view.

3. Prediction of enhanced scour

A simple model for pore-pressure field, p, is the one by Terzaghi (1925):

$$\frac{\partial p}{\partial t} = c_v \frac{\partial^2 p}{\partial z^2}, \tag{2}$$

where c_v is Terzaghi's consolidation coefficient: $c_v = \frac{k}{\rho g}\frac{1+e_0}{a_v}$, where k is the hydraulic conductivity in Darcy's Law, ρ is the liquid density, e_0 is the voids ratio at the initial time, a_v is the coefficient of compressibility, i.e. $a_v = -de/d\sigma$, σ is the effective stress. Equation (2) is a representation of the conservation of mass in terms of pressure with the use of Darcy's law and the soil compressibility resulted from the change in void ratio. It was developed to estimate the foundation settlement that a relatively impermeable layer (e.g. clay) will undergo before it reaches equilibrium with the external load. Hence, (2) is usually applied for the situations for much longer time scale phenomena with much smaller values of c_v than the present scouring situation in sandy soils.

For tsunami-induced scour, Tonkin et al. (2003) hypothesized that as the water level subside, the pressure on the sediment bed decreases, creating a vertical pressure gradient and decreasing the effective stress within the soil. They used the exact analytical solution to (2) for infinite soil thickness assuming that the surface pressure decreases linearly from a sustained peak at ΔP to zero over time ΔT. They combined the analytical solution with the soil stability condition given by the pore-pressure gradient and yielded the quantitative prediction for the movable soil depth, d_s, of tsunami-induced scour:

$$d_s = \frac{\Delta P}{\gamma_b \Lambda}\left(1 - 4\mathrm{i}^2\mathrm{erfc}\left[\frac{d_s}{2\sqrt{c_v \Delta T}}\right]\right) \tag{3}$$

where Λ is the fraction of the buoyant weight of soil supported by the pore pressure gradient, γ_b is the buoyant specific weight of the saturated soil skeleton, and $\mathrm{i}^2\mathrm{erfc}[\bullet]$ is the second integral of the complementary error function. Note that d_s is implicit in (3) and $\Lambda = 1$ represents zero effective stress condition at depth = d_s. The limiting condition of $d_s \rightarrow 0$ yields a measure of whether any soil instability due the pore-pressure gradient can occur:

$$\Lambda = \frac{2}{\sqrt{\pi}}\frac{\Delta P}{\gamma_b \sqrt{c_v \Delta T}}. \tag{4}$$

4. Determination of c_v

Consolidation is the process whereby pore pressure is dissipated within a soil resulting in compression of the soil skeleton. In fine-grained soils (clay) this process takes a long time (days to years). In coarse-grained soils (sand) the pore size is large enough that the water flow and pore pressure dissipation can occur in a matter of seconds or minutes. On the time scale of typical construction projects this time scale is practically instantaneous. For this reason very little effort has been made to evaluate c_v for sands. Table 2 provides a list of c_v values for fine- and coarse-grained soils. The table shows the wide variation in c_v of sands: 10 ~ 10,000 cm^2/s! It is noted that the standard oedometer tests may not be suitable to evaluate the high value of c_v. Instead, we used an apparatus that mimics the rapid pressure relief on the soil surface in a controlled manner, allowing the values of c_v to be determined by (2) with the direct measurements of pore-pressure field.

Table 2: Select list of c_v values for fine- and coarse-grained soils. 1. Al-Dhahir & Tan, 1968; 2. Holtz & Kovaks, 1981; 3. Mitchell, 1992; 4. Nash & Ryde, 2001; 5. Sridharan & Prakash, 2001; 6. Sridharan et al, 1995; 7. Ward et al, 1959; 8. Zen & Yamazaki, 1990; 9. Zen & Yamazaki, 1991

Soil Name	c_v (cm^2/s)		Source
	Range	Average	
Montmorillonite	0.000006 - 0.00003	0.000018	3
London Clay	0.000094 - 0.000136	0.000115	1
Mexico City CLAY	0.00009 - 0.00015	0.00012	2
San Fransisco Bay Mud	0.0002 - 0.0004	0.0003	2
Chicago Clay	0.00034 - 0.00054	0.00044	6
London CLAY	0.0001 - 0.0009	0.0005	7
Organic SILT	0.0002 - 0.0010	0.0006	2
Chicagoo Silty CLAY	0.00085	0.00085	2
Koalinite	0.0021 - 0.0049	0.0035	6
Boston Blue CLAY	0.0020 - 0.0060	0.004	3
Kaolinite & Montmorillonite	0.003 - 0.1	0.0515	5
Kaolinite	0.01 - 1.0	0.505	5
Red Earth-1 (Kaolinite)	0.0007 - 0.2	0.1	5
Toyoura SAND (D_{50}=0.181mm)	12	12	8
Poorly Graded Beach Sand (D_{50}=0.35mm)	80	80	7
Sitly SAND	150 - 1500	824	4
Hazaki SAND (D_{50}=0.16mm)	7180	7180	9
Poorly Graded Beach Sand (D_{50}=0.35mm)	10000	10000	9
Hazaki SAND (D_{50}=0.16mm)	11520	11520	9

Figure 6 depicts the apparatus that consists of a vertical specimen column, 1 m high, 10 cm in diameter, and the upper and lower headpipes, 25mm diameter. Seven pressure ports are positioned vertically in the column – only five ports were used for the present tests. Three were placed in the soil specimen in 16.6 cm interval, one in the water above the specimen and one in the water below the specimen. The pressure transducers are attached at the end of stainless steel tubing with a 90° bend upward on the outside of the specimen and a porous plastic at the sand interface. The bend allows for air to be flushed out from the system helping to ensure saturation. A ball valve and a flow-regulation orifice are located at the top of the column as the controlled pressure relief devises. The specimen is prepared using wet pluviation to ensure saturation and low relative density of the specimen (Vaid & Negussey, 1988). The sand used is an Ottawa Fine Sand with D_{50} = 0.26mm. A constant pressure head is maintained to the base of the specimen via the lower headpipe, and opening the ball valve decreases the pressure at the top of the specimen. This simulates the drawdown phase of a tsunami type wave, but without shear stresses induced by the flow.

Typical test data are shown in Fig. 7. Only clean data during the initial pressure relief are used for the analysis: indicated by "time window" in Fig. 7. The value of c_v is evaluated by (2) from the temporal and spatial variations of the pore-pressures. As seen in Fig. 7b, the value of c_v decreases in time. The reason is not clear, but it may relate to an increase in the coefficient of compressibility, a_v with an increase in the soil voids ratio. We tested 14 different cases varying the initial void ratios from 0.56 to 0.77, and three pressure relief rates. The average value of c_v was found to be 750 cm^2/s, with a range from 400 to 1200 cm^2/s; more detailed results can be found in Heller (2002).

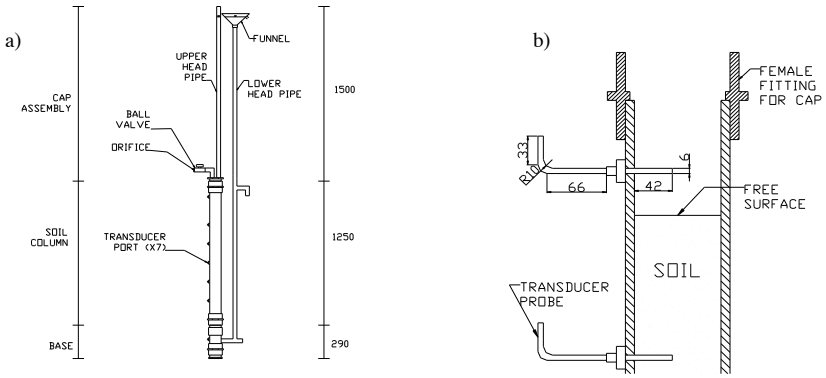

Figure 6. a) Schematic of testing device. b) Cross section of upper portion of soil column. Note that probes reach to center of soil specimen. All dimensions in mm.

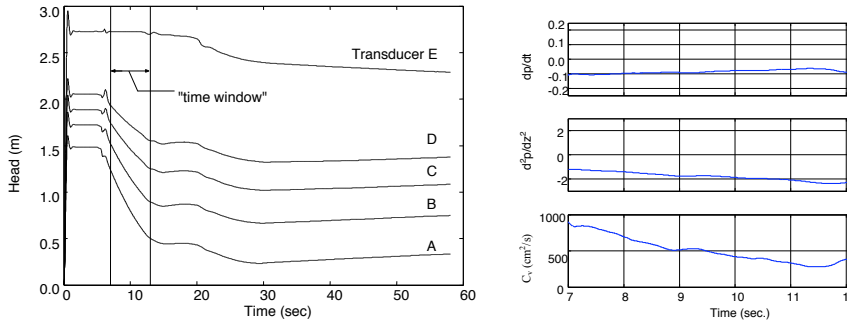

Figure 7. a) Typical pore-pressure test data. b) Evaluation of C_v, from the data in the time window based on (2)

5. Discussion and conclusions

Scour depths at the terminal stage of the laboratory experiments (Fig. 5) were analyzed with (3) and (4), using the value c_v = 750 cm^2/s, and the results are shown in Table 3. The results indicate that $\Lambda(0)$ lies below 0.5 for those cases where relatively shallow scour holes are formed; $\Lambda(0)$ lies slightly above 0.5 for the three cases where a deep scour is observed during drawdown. This suggests that significant soil instability results when Λ exceeded one-half for their experiments on scour around a vertical cylinder. Malvick et al. (2003) explained the similar phenomena that the critical value of Λ (or the pore pressure ratio, r_u) during triggering of liquefaction-induced flow slides is limited by the Mohr-Coulomb failure criteria such that Λ linearly decreases with static shear stress.

The criteria (3) and (4) appear useful for the prediction of tsunami scour. Once tsunami runup-drawdown being estimated (perhaps with a numerical computation), ΔP and ΔT can be evaluated. The problem, however, remains due to the uncertainty in the value of consolidation coefficient c_v, which does not appear constant.

Table 3: Calculation of the scour enhancement parameter

h (m)	H (m)	ΔT (s)	ΔP (kPa)	$\Lambda(0)$	Measured scour depth d_s (m)	$\Lambda(d_s)$
2.65	0.13	4.5	1.28	0.26	0.000	-
2.65	0.24	6.5	1.77	0.30	0.025	-
2.65	0.34	6.0	1.96	0.35	0.043	-
2.45	0.22	3.0	1.37	0.35	0.024	-
2.65	0.13	4.5	1.67	0.35	0.026	-
2.65	0.24	6.5	3.34	0.57	0.144	0.52
2.65	0.34 [1]	6.5	3.63	0.62	> 0.2	< 0.55
2.45	0.22 [2]	6.5	3.34	0.57	0.145	0.52

References

Al-Dhahir, Z.A. and D.I.C. Tan (1968) "A Note on One-Dimensional Constant-Head Permeability Tests," *Geotechnique*. 18 (4) 499-505

Heller, E.W. (2003). "Determination of the diffusion coefficient for sands for the prediction of enhanced scour on beaches due to tsunamis," Master's Thesis, University of Washington, Department of Civil and Environmental Engineering, Seattle, Washington.

Hoffmans, G.J.C.M. and H.J. Verheij (1997). *Scour Manual*. A.A. Balkema, Rotterdam.

Holtz, R.D and W.D. Kovacs, (1981). "Derivation and solution of Terzaghi's one-dimensional consolidation theory," In *An Introduction to Geotechnical Engineering*, 683-690, Prentice Hall, Englewood Cliffs, NJ.

Malvick, E.J., Kulasingam, R. , Boulanger, R. W., Kutter, B.L. (2003). "Analysis of a Void Redistribution Mechanism in Liquefied Soil" in Proc. 12th Panam. Conf. on Soil Mech. & Geotechnical Eng., Cambridge, MA, Verlag Glückauf GMBH, Essen, Germany (ed: Culligan, Einstein, and Whittle), pp. 955-961

Mitchell, J. K. (1993). *Fundamentals of Soil Behavior*, John Wiley & Sons, New York.

Nash, D.F.T. and S.J. Ryde, (2001). "Modeling Consolidation Accelerated by Vertical Drains in Soils Subject to Creep," *Geotechnique*, 51 (3) 257-273.

Sridharan,A. and K. Prakash, (2001). "Consolidation and permeability behavior of segregated and homogeneous soils," *Geotechnical Testing Journal*, 21 (1) 109-120.

Sridharan,A., K. Prakash and S.R. Asha, (1995). "Consolidation behavior of soils," *Geotechnical Testing Journal*, 18 (1) 58-68.

Takahashi T., Imamura, F. and Shuto, N. (1992). "Research on flows and bathymetry variations by tsunami: the Case of Kesen-numa Bay, Japan, due to the 1960 Chilean Tsunami" (in Japanese). Tsunami Engineering Technical Report No. 9, Tohoku University, 185-201.

Terzaghi, K. (1925). *Erdbaumechanik* (in German). Franz Deutike, Vienna.

Tonkin, S., Yeh, H., Kato, F., and Sato S. (2003). "Tsunami Scour around a Cylinder: an Effective Stress Approach," *Journal of Fluid Mechanics*, 496, 165-192.

Vaid, Y.P. and D. Negussey, (1988). "Preparation of reconstituted sand specimens," In *Advanced triaxial testing of soil and rock*, *ASTM STP 977*, R. T. Donaghe, R. C. Chaney, and M. L. Silver, Eds., 405-417, ASTM, Philadelphia.

Ward, W.H., S.G. Samuels, and M.E. Butler, (1959). "Further studies of the properties of London Clay," *Geotechnique*, 9 (2) 33-58.

Zen, K., and H. Yamazaki, (1990). "Oscillatory pore pressure and liquefaction in seabed induced by ocean waves," *Soils and Foundations*, 30, 147-161.

Zen, K., and H. Yamazaki, (1991). "Field observation and analysis of wave-induced liquefaction in seabed," *Soils and Foundations,* 31: 161-179.